Indian Journal of Pure & Applied Physics
Vol. 61, November 2023, pp. 897-902
DOI: 10.56042/ijpap.v61i11.2450

Self-Focusing and Defocusing of Lorentz-Gauss Laser Beam in Collisionless Plasma

Prajakta P Patil[a], S D Patil[a*] & M V Takale[b]

[a]Department of Physics, Devchand College, Arjunnagar, Maharashtra 591 237, India

[b]Department of Physics, Shivaji University, Kolhapur, Maharashtra 416 004, India

Received 12 June 2023; accepted 28 August 2023

The propagation of Lorentz-Gauss (L-G) Laser beam in collisionless plasma is investigated. Based on WKB and paraxial approximations, coupled differential equations for beam-width parameters in two transverse dimensions of L-G beam are derived under the parabolic equation approach. The self-focusing and self-defocusing characters of L-G beam are numerically demonstrated. The influence of Lorentz width on the propagation of L-G beam through plasma is specifically considered. It is found that the heterogeneous intensity distribution of L-G beam plays a vital role in its propagation dynamics through plasmas.

Keywords: Lorentz-Gauss; Self-focusing; Collisionless plasma

1 Introduction

The nonlinear propagation of laser through plasmas has remarkable application domains in many regimes such as laser-based inertial confinement fusion schemes[1-3], laser-influenced electron acceleration[4-6], harmonic generation[7-12] and generation of new radiation sources[13,14]. Most of these applications are generally based on the long-distance propagation of lasers. However, due to the dominance of diffraction, laser beam propagation is limited over several Rayleigh lengths through plasma. Therefore, the phenomenon of self-focusing[15] of laser beam in plasma plays a very crucial role in the field of laser-plasma interaction. Self-focusing in plasmas is a nonlinear optical phenomenon that appears due to the wave front distortion inflicted on the beam by itself while traversing plasma. Such distortion is due to the changes in the dielectric constant of the plasma arising from the high intensity of the laser beam with a non-uniform transverse spatial extent. It sometimes plays a vital role in affecting other nonlinear phenomena[16].

Before proceeding further, it is instructive to consider the nonlinearities responsible for focusing in plasmas[17]. There are three main nonlinearities in the dielectric constant, viz., collisional, ponderomotive and relativistic, which are, in fact, operative for the appearance of self-focusing of laser. In collisional plasmas, the electrons get heated to different temperatures in the transverse plane on account of the radial distribution of the field of the beams. In the steady state, the distribution of electron temperature is determined by the Ohmic heating and the power loss by collisions and thermal conduction. This causes a radial redistribution of electron density and, thereby the dielectric constant[18]. For collisionless plasma, the ponderomative force on electrons is proportional to the gradient of irradiance of the beam. This causes the redistribution of electron density and, thereby, the dielectric constant[19]. For high powers of the beams, the quiver velocity of the electrons is comparable to the speed of light in a vacuum. The radial distribution of irradiance of the beam causes a corresponding redistribution of the electron mass and hence dielectric constant[20]. The form of nonlinear dielectric constant is different in different physical situations of plasma, but its dependence on irradiance of the beam is a common feature.

In the phenomenon of self-focusing, the salient features of the fundamental Gaussian laser beam are advantageous in simplifying the mathematical complexities involved in the theoretical treatment of various nonlinear phenomena. A study of the literature reveals that past studies on the self-action effects of laser beams in plasmas were mostly concerned with revealing the dynamics of Gaussian laser beams or laser beams with irradiance that is

*Corresponding author: (E-mail: sdpatil_phy@rediffmail.com)

close to Gaussian. On the other hand, it is also important from a practical point of view that certain laser sources produce fields that show variations in Gaussian distribution. It is well-known that though the Gaussian beam exploits a minimum uncertainty field, it possesses the minimum achievable angular spreading once the spatial extension is fixed for certain laser sources. For this purpose, lasers are utilized in different capacities in plasmas with variety of configurations, e.g. elliptic Gaussian beams[21,22], cosh-Gaussian beams[23-27], Hermite-Gaussian beams[28,29], Bessel-Gaussian beams[30-32], q-Gaussian beams[33-36], quadruple Gaussian beams[37-39], skewed beams[40-42], Airy-Gaussian beams[43-45], Laguerre-Gaussian beams[46-48], Hermite-cosine Gaussian beams[49,50] etc. have been attempted in recent years.

With the development of lasers, a new laser beam profile called Lorentz-Gaus (L-G) beam[51,52] has been introduced. In the same spatial extension, the angular spread of the L-G beam is higher than that of a Gaussian beam. A simple mathematical representation of such field distribution resembles the combined Gaussian and Lorentzan functions[53]. This kind of beam can exhibit heterogeneous distribution, such as distorted wave front or asymmetric field distribution as well as unevenly distributed spots in the context of transverse dimensions of the beam. To our knowledge, propagation characters of the L-G beam in plasma have not been reported. As a result, the L-G beam will invite extensive studies in the growing field of laser-plasma interaction. The purpose of the present paper is to examine the nonlinear propagation of the L-G beam in plasma.

2 Theoretical Formulation

In a Cartesian coordinate system, the electric field distribution of L-G beam at $z = 0$ plane can be described by[51]

$$E(x, y, z = 0) = E_0 \, exp\left(-\frac{x^2}{r_0^2}\right) \frac{1}{\left[1+\left(\frac{y}{\delta \gamma_0}\right)^2\right]}, \qquad (1)$$

where E_0 is the constant amplitude, parameters r_0 and γ_0 are the widths of Gaussian and Lorentzian distributions, respectively, δ is the dimensionless adjustable parameter. This kind of field has the product of two functions of x and y variables, which have the form of Gaussian function of parameter r_0 and Lorentzian function of parameter γ_0, respectively. Fig 1 depicts the initial beam profiles with their above orthographic views for two values of δ parameter. We have kept two different δ values ($\delta = 0.5$ and $\delta = 2.0$). From this figure, heterogeneity in intensity distribution through δ parameter of the beam is observed.

The effective dielectric function of the plasma can, in general, be expressed as[15]

$$\varepsilon = \varepsilon_0 + \Phi(EE^*), \qquad (2)$$

where $\varepsilon_0 = 1 - \left(\omega_p^2/\omega^2\right)$ is the linear part of ε with $\omega_p = (4\pi n_0 e^2/m)^{1/2}$. Here, ω is the frequency of the laser, n_0 is the plasma density of electrons in the absence of the beam, e and m are the electronic charge and mass of electron, respectively. In the case of ponderomotive nonlinearity in collisionless plasma, the nonlinear part $\Phi(EE^*)$ is written as[17]

$$\Phi(EE^*) = \frac{\omega_p^2}{\omega^2}\left[1 - exp\left(-\frac{3}{4}\frac{m}{M}\beta EE^*\right)\right], \qquad (3)$$

where $\beta = e^2/8m^2\omega^2 k_B T_0$ is the coefficient of ponderomative nonlinearity, M is the mass of the ion, k_B is Boltzmann's constant and T_0 is the equilibrium plasma temperature.

When we assume a time dependence of the electric field, $E \sim exp(i\omega t)$, and ignore the term $\nabla(\nabla \cdot E)$, which is justified if $(c^2/\omega^2)|(1/\varepsilon)\nabla^2 \ln \varepsilon| \ll 1$, the time-independent scalar wave equation takes the form

$$\nabla^2 E + \frac{\omega^2}{c^2}\varepsilon E = 0. \qquad (4)$$

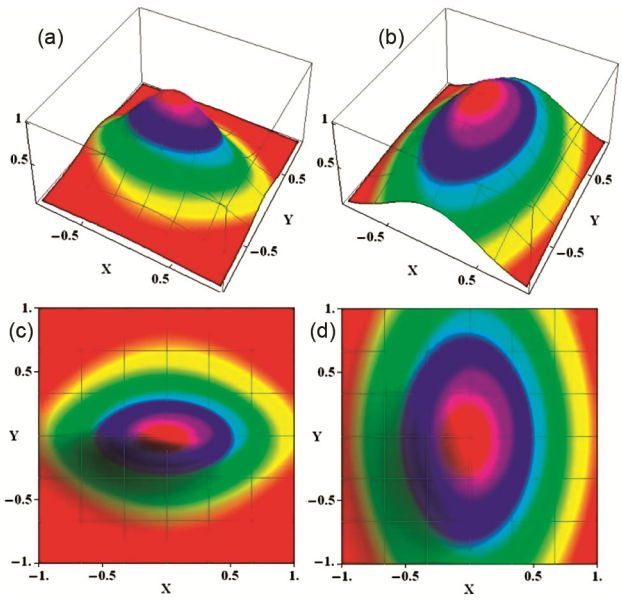

Fig 1 — 3D intensity profile of L-G beam for (a) $\delta = 0.5$ and (b) $\delta = 2.0$. The transverse view of intensity profile are (c) $\delta = 0.5$ and (d) $\delta = 2.0$.

When we assume that $E = A(x,y,z)exp(-ikz)$ and employ the WKB approximation, Eq. (4) yields

$$-2ik\frac{\partial A}{\partial z} + \nabla_{\perp}^2 A + k^2\frac{\Phi(AA^*)}{\varepsilon_0}A = 0, \quad (5)$$

where $k = (\omega/c)\sqrt{\varepsilon_0}$ is the wave propagation vector.

Substituting $A = A_0\, exp[-ikS(x,y,z)]$ into Eq. (5) and separating real and imaginary parts, one obtains

$$2\frac{\partial S}{\partial z} + \left(\frac{\partial S}{\partial x}\right)^2 + \left(\frac{\partial S}{\partial y}\right)^2 = \frac{1}{k^2 A_0}\nabla_{\perp}^2 A_0 + \frac{\Phi(A_0 A_0^*)}{\varepsilon_0},$$

$$\frac{\partial A_0^2}{\partial z} + \frac{\partial S}{\partial x}\frac{\partial A_0^2}{\partial x} + \frac{\partial S}{\partial y}\frac{\partial A_0^2}{\partial y} + A_0^2\nabla_{\perp}^2 S = 0. \quad (6)$$

The solutions of Eqs.(6) can be written as

$$A_0^2 = \frac{E_0^2}{f_1 f_2}\, exp\left(-\frac{2x^2}{r_0^2 f_1^2}\right)\frac{1}{\left[1+\left(\frac{y}{\delta\gamma_0 f_2}\right)^2\right]^2},$$

$$S = \frac{x^2}{2f_1}\frac{df_1}{dz} + \frac{y^2}{2f_2}\frac{df_2}{dz} + \varphi(z) \quad (7)$$

where f_1 and f_2 are the dimensionless beam-width parameters in x and y dimensions of the beam respectively.

Substituting A_0 and S in Eq. (6), using the paraxial approximation and separately equating coefficients of x^2 and y^2 on both sides of the resulting equation, one obtains

$$\frac{d^2 f_1}{d\zeta^2} = \frac{4}{f_1^3} - 2\left(\frac{r_0\omega_p}{c}\right)^2\frac{\alpha E_0^2}{f_1^3 f_2^2}\, exp\left(-\frac{\alpha E_0^2}{f_1 f_2}\right),$$

$$\frac{d^2 f_2}{d\zeta^2} = \frac{10}{f_2^3}\left(\frac{r_0}{\delta\gamma_0}\right)^4 - 2\left(\frac{r_0\omega_p}{c}\right)^2\left(\frac{r_0}{\delta\gamma_0}\right)^2\frac{\alpha E_0^2}{f_2^3 f_1^2}\, exp\left(-\frac{\alpha E_0^2}{f_1 f_2}\right). \quad (8)$$

where αE_0^2 is the initial intensity parameter with $\alpha = 3m\beta/4M$ and $\zeta = z/R_d$ is the dimensionless distance of propagation with $R_d = kr_0^2$ as the Rayleigh's diffraction length. The initial conditions on f_1 and f_2 are:

$$f_1(\zeta = 0) = 1, \left(\frac{df_1}{d\zeta}\right)_{\zeta=0} = 0$$

$$f_2(\zeta = 0) = 1, \left(\frac{df_2}{d\zeta}\right)_{\zeta=0} = 0 \quad (9)$$

For an initially plane wavefront of the beam corresponding to $d^2 f_1/d\zeta^2 = 0$, $f_1 = 1$ and $d^2 f_2/d\zeta^2 = 0$, $f_2 = 1$ at $\zeta = 0$, the critical values of E_0^2 for self-trapping in x and y dimensions of the beam are obtained from Eqs. (8) as

$$\alpha E_{0crx}^2 exp(-\alpha E_{0crx}^2) = \frac{2c^2}{r_0^2\omega_p^2}$$

$$\alpha E_{0cry}^2 exp\left(-\alpha E_{0cry}^2\right) = \frac{5c^2}{\delta^2\gamma_0^2\omega_p^2} \quad (10)$$

where E_{0crx} and E_{0cry} are critical values of electric field for self-trapping of L-G beams in x and y dimensions of the beam respectively.

3 Results and Discussion

Equations (8) are second-order, ordinary, nonlinear and coupled differential equations for beam-width parameters, f_1 and f_2 that determines the width of the L-G beam in respective x and y dimensions of the beam. These equations are not integrable and hence we require a suitable numerical technique to solve them. In the present paper, we have solved these equations by using the Runge-Kutta fourth-order method under the initial conditions given by Eqs. (9). Eqs. (8) simply deals with diffraction by letting the term $\Phi \to 0$ in Eq. (6). Because of nonlinearity Φ in Eq. (6), the evolution of beam-width parameters f_1 and f_2 on the left-hand side of Eqs. (8) is determined by the relative competition between the magnitude of two terms on their right-hand sides. When the magnitude of the first term (diffraction term) is greater than that of the second term (nonlinear term) in each Eq. (8), $d^2 f_1/d\zeta^2$ and $d^2 f_2/d\zeta^2$ becomes positive and hence f_1 and f_2 increase with ζ, i.e. the defocusing of the beam is sure in both x and y directions. In the reverse case, it clearly promises self-focusing. If the terms on the right-hand sides of Eqs. (8) cancel each other, then the beam propagates without change in its profile, i.e. the beam neither focuses nor defocuses. This is usually known as the self-trapped mode (uniform waveguide mode) of the beam in the medium. It is interesting to note in the present case of nonlinear L-G beam propagation through collisionless plasma, self-focusing/defocusing of the L-G beam depends on width parameters r_0 and γ_0 of Gaussian and Lorentzian distributions.

We define a critical value of E_0^2 as E_{0cr}^2 in Eqs. (10) for each dimension respectively, for which two terms on the right-hand sides of Eqs. (8) cancel each other. It is found that each of the Eqs.(10) gives two roots as E_{0crx1}^2, E_{0crx2}^2 $(E_{0crx1}^2 < E_{0crx2}^2)$ and E_{0cry1}^2, E_{0cry2}^2 $(E_{0cry1}^2 < E_{0cry2}^2)$. Also, both E_{0crx}^2 and E_{0cry}^2 increases with decreasing $r_0\omega_p/c$ and $\gamma_0\omega_p/c$. At $r_0/\gamma_0 = \sqrt{2/5}\ \delta$, both $E_{0crx1} = E_{0cry1}$ and $E_{0crx2} = E_{0cry2}$. The magnitude of four critical field values gives an

inequality condition as, $E_{0crx1}^2 < E_{0cry1}^2 < E_{0cry2}^2 < E_{0crx2}^2$. We have solved Eqs. (8) subject to the initial conditions given by Eqs. (9) in the case of collisionless plasma. To have a numerical assessment, we have used Ti: sapphire laser of wavelength $\lambda = 800\,nm$ with initial intensity $I{\sim}10^{17}\,Wcm^{-2}$. The typical values of other numerical laser-plasma parameters used for computation are: $r_0 = 20\,\mu m$, $\gamma_0 = 20\,\mu m$, $n_0 = 10^{19}\,cm^{-3}$, $T_0 = 10^5\,K$, $\delta = 0.5$ and 2.0. The variations of beam-width parameters f_1 and f_2 with dimensionless distance of propagation ζ are shown for regions corresponding to the following five cases:

(i) $E_0^2 < E_{0crx1}^2 < E_{0cry1}^2 < E_{0cry2}^2 < E_{0crx2}^2$
(ii) $E_{0crx1}^2 < E_0^2 < E_{0cry1}^2 < E_{0cry2}^2 < E_{0crx2}^2$
(iii) $E_{0crx1}^2 < E_{0cry1}^2 < E_0^2 < E_{0cry2}^2 < E_{0crx2}^2$
(iv) $E_{0crx1}^2 < E_{0cry1}^2 < E_{0cry2}^2 < E_0^2 < E_{0crx2}^2$
(v) $E_{0crx1}^2 < E_{0cry1}^2 < E_{0cry2}^2 < E_{0crx2}^2 < E_0^2$

Figure 2 represents the variation of f_1 and f_2 with ζ in the region corresponding to $E_0^2 < E_{0crx1}^2 < E_{0cry1}^2 < E_{0cry2}^2 < E_{0crx2}^2$, with $\alpha E_0^2 = 0.005$ and $\alpha E_0^2 = 0.0001$ beam diverges in both x and y dimensions for both $\delta = 0.5$ and $\delta = 2.0$ cases. It is observed from this figure that the steady defocusing rate of f_2 is greater than that of f_1 for $\delta = 0.5$ as shown by thick curves. In the opposite case, such a defocusing rate of f_2 is less than that of f_1 for $\delta = 2.0$. The similar behaviour of f_1 and f_2 with ζ is observed for the region corresponding to $E_{0crx1}^2 < E_0^2 < E_{0cry1}^2 < E_{0cry2}^2 < E_{0crx2}^2$ for both cases of $\delta = 0.5$ and $\delta = 2.0$ with $\alpha E_0^2 = 0.05$ and $\alpha E_0^2 = 0.001$ as shown in Fig. 3. From Fig. 4, it is clear that complexity in the oscillatory character of f_1 and f_2 with ζ is observed for $\alpha E_0^2 = 2$ and $\alpha E_0^2 = 3$ with $\delta = 0.5$ and $\delta = 2.0$ respectively, in the region

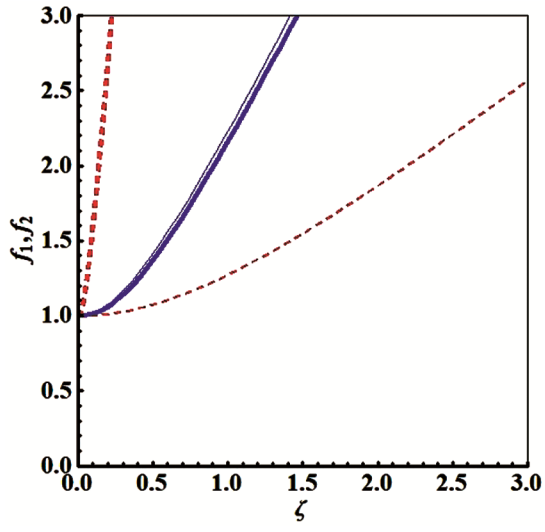

Fig 2 — Variation of f_1 and f_2 with ζ in collisionless plasma for initial intensity parameter $\alpha E_0^2 = 0.005$ with $\delta = 0.5$ (thick curves) and $\alpha E_0^2 = 0.0001$ with $\delta = 2$ (thin curves). Solid curves are for f_1 and dashed curves are for f_2. The numerical values of laser-plasma parameters used are: $\lambda = 0.8\,\mu m$, $r_0 = 20\,\mu m$, $\gamma_0 = 20\,\mu m$, $n_0 = 10^{19}\,cm^{-3}$, $T_0 = 10^5\,K$.

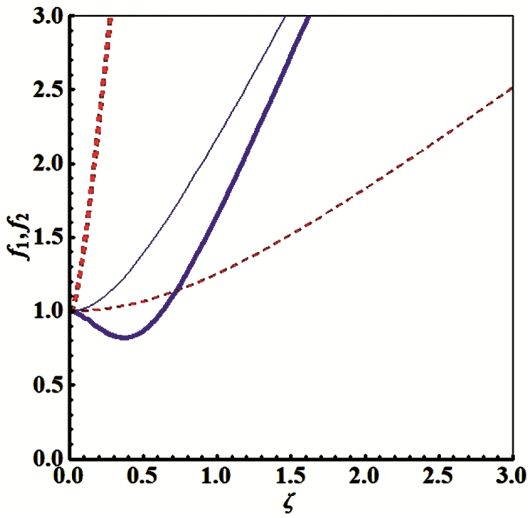

Fig 3 — Variation of f_1 and f_2 with ζ in collisionless plasma for initial intensity parameter $\alpha E_0^2 = 0.05$ with $\delta = 0.5$ (thick curves) and $\alpha E_0^2 = 0.001$ with $\delta = 2$ (thin curves). Solid curves are for f_1 and dashed curves are for f_2. The numerical values of the laser-plasma parameter are the same as that of Figure 2.

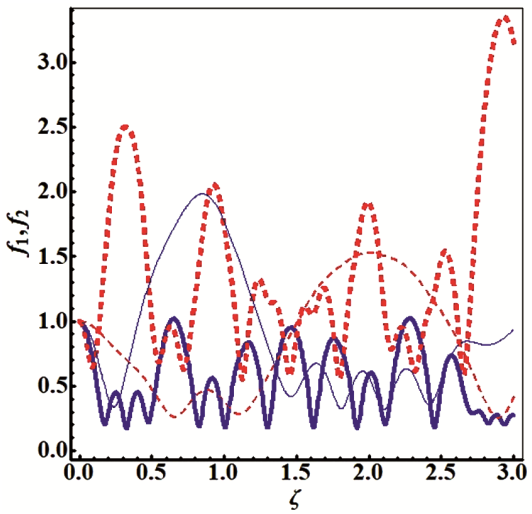

Fig 4 — Variation of f_1 and f_2 with ζ in collisionless plasma for initial intensity parameter $\alpha E_0^2 = 2$ with $\delta = 0.5$ (thick curves) and $\alpha E_0^2 = 3$ with $\delta = 2$ (thin curves). Solid curves are for f_1 and dashed curves are for f_2. The numerical values of the laser-plasma parameter are the same as that of Figure 2.

corresponding to $E_{0crx1}^2 < E_{0cry1}^2 < E_0^2 < E_{0cry2}^2 < E_{0crx2}^2$. It is also observed that after initial focusing of the beam in both x and y dimensions, x dimension of the beam focuses while y dimension defocuses in an oscillatory manner.

In Fig. 5, the variation of f_1 and f_2 with ζ is oscillatory for both $\alpha E_0^2 = 4$ and $\alpha E_0^2 = 6.3$ with $\delta = 0.5$ and $\delta = 2.0$ respectively, in region $E_{0crx1}^2 <$

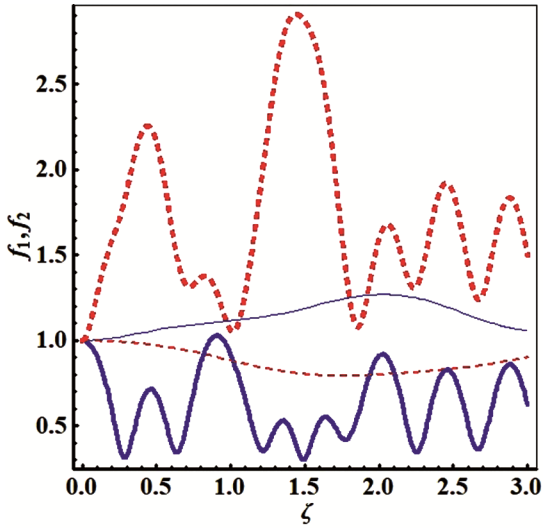

Fig 5 — Variation of f_1 and f_2 with ζ in collisionless plasma for initial intensity parameter $\alpha E_0^2 = 4$ with $\delta = 0.5$ (thick curves) and $\alpha E_0^2 = 6.3$ with $\delta = 2$ (thin curves). Solid curves are for f_1 and dashed curves are for f_2. The numerical values of laser-plasma parameter are same as that of Figure 2.

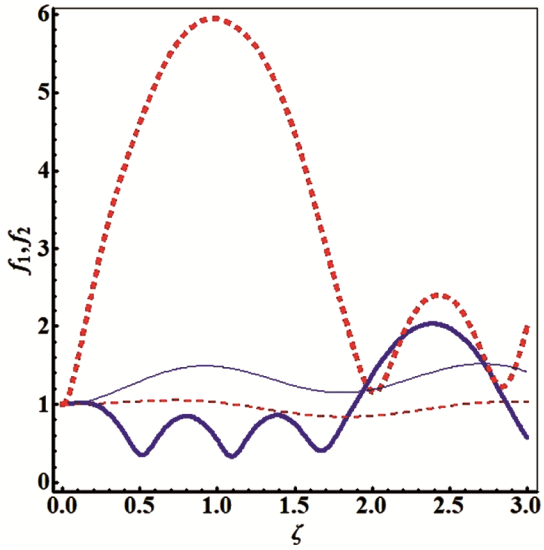

Fig 6 — Variation of f_1 and f_2 with ζ in collisionless plasma for initial intensity parameter $\alpha E_0^2 = 8$ with $\delta = 0.5$ (thick curves) and $\alpha E_0^2 = 8$ with $\delta = 2$ (thin curves). Solid curves are for f_1 and dashed curves are for f_2. The numerical values of the laser-plasma parameter are the same as that of Figure 2.

$E_{0cry1}^2 < E_{0cry2}^2 < E_0^2 < E_{0crx2}^2$. Focusing of f_1 leads to the defocusing of f_2 for $\delta = 0.5$, as shown by thick curves. However, a reverse trend is preserved with a reduction in the oscillation amplitude of f_1 and f_2 with ζ in the case of $\delta = 2.0$ as depicted by thin curves. Similar variation of f_1 and f_2 with ζ is also observed in Fig. 6 for the region $E_{0crx1}^2 < E_{0cry1}^2 < E_{0cry2}^2 < E_{0crx2}^2 < E_0^2$ with $\alpha E_0^2 = 8$ ($\delta = 0.5$) and $\alpha E_0^2 = 8$ ($\delta = 2.0$). The width parameters f_1 and f_2 vary in a periodic manner with a reduced number of oscillations during propagation through plasma.

4 Conclusion

In conclusion, the self-focusing/defocusing of the L-G beam in collisionless plasma is studied. Coupled differential equations for beam-width parameters in two transverse dimensions of the L-G beam are derived. The study concludes that the self-focusing of the L-G beam depends on regions corresponding to different critical values of electric fields. The asymmetric self-focusing/defocusing of the L-G beam is observed due to the heterogeneous distribution of intensity along transverse dimensions of the L-G beam. The present study may be useful to characterize heterogeneous field distribution of laser beams in various situations of plasma, which, however, to the best of our knowledge, have not been attempted extensively in the literature at present.

References

1 Betti R & Hurricane O A, *Nature Phys*, 12 (2016) 435.
2 Qian Y & Huang B, *J Phys: Conf Ser*, 2108 (2021) 012095.
3 Schmitt A J & Obenschain S P, *Phys Plasmas*, 30 (2023) 012701.
4 Ghotra H S & Kant N, *Laser Part Beams*, 34 (2016) 385.
5 Ghotra H S & Kant N, *Phys Plasmas*, 23 (2016) 053115.
6 Kant N, Rajput J & Singh A, *High Energy Density Phys*, 26 (2018) 16.
7 Kant N & Thakur V, *Optik* 127 (2016) 4167.
8 Thakur V & Kant N, *Laser Part Beams* 36 (2018) 363.
9 Walia K, Kakkar V & Tripathi D, *Optik*, 204 (2020) 164150.
10 Walia K, Verma R K & Singh A, *Optik*, 225 (2021) 165745.
11 Kakkar V, Walia K & Tripathi D, *Optik*, 226 (2021) 165978.
12 Kakkar V, Walia K & Tripathi D, *Optik*, 244 (2021) 167597.
13 Buldt J, Mueller M, Stark H, Jauregui C & Limpert J, *Appl Phys B*, 126 (2020) 2.
14 Butorin P S, Kalmykov S G, Maximov V A & Sasin M E, *J Phys: Conf Ser*, 1697 (2020) 012237.
15 Akhmanov S A, Sukhorukov A P & Khokhlov R V, *Sov Phys Usp*, 10 (1968) 609.
16 Agarwal S K & Sodha M S, *Optik* 118 (2007) 367.
17 Sodha M S, Ghatak A K & Tripathi V K, *Prog Opt*, 13 (1976) 169.
18 Sodha M S & Sharma A, *J Plasma Phys*, 70 (2008) 473.
19 Wani M A & Kant N, *Optik*, 127 (2016) 4705.

20 Zhang G, Liang Q & Xia X, *Laser Part Beams*, 38 (2020) 244.
21 Kumar H, Aggarwal M & Gill T S, *J Opt Soc Am B*, 35 (2018) 1635.
22 Walia K & Tripathi D, *Optik*, 186 (2019) 46.
23 Vhanmore B D, Patil S D, Valkunde A T, Urunkar T U, Gavade K M & Takale M V, *Laser Part Beams*, 35 (2017) 670.
24 Urunkar T U, Patil S D, Valkunde A T, Vhanmore B D, Gavade K M & Takale M V, *Commun Theor Phys*, 70 (2018) 220.
25 Nanda V, Ghotra H S & Kant N, *Optik*, 156 (2018) 191.
26 Walia K & Singh A, *Optik*, 247 (2021) 167867.
27 Walia K, Singh T & Singh A, *Optik*, 258 (2022) 168894.
28 Kant N, Wani M A & Kumar A, *Opt Commun*, 285 (2012) 4483.
29 Sharma V, Thakur V & Kant N, *Optik*, 194 (2019) 163076.
30 Patil S D, Valkunde A T, Vhanmore B D, Urunkar T U, Gavade K M & Takale M V, *AIP Conf Proc*, 2142 (2019) 110012.
31 Patil S D, Vhanmore B D & Takale M V, *J Opt*, 49 (2020) 510.
32 Patil S D, Vhanmore B D & Takale M V, *J Russ Laser Res*, 42 (2021) 45.
33 Vhanmore B D, Patil S D, Valkunde A T, Urunkar T U, Gavade K M, Takale M V & Gupta D N, *Optik*, 158 (2018) 574.
34 Khandale K Y, Takale P T, Urunkar T U, Patil S S, Nikam P P, Mane M B, Pawar V S, Valkunde A T, Patil S D & Takale M V, *Bulg J Phys*, 49 (2022) 375.
35 Walia K, *Optik*, 277 (2023) 170681.
36 Butt A A, Kant N & Thakur V, *Phys Scr*, 98 (2023) 045621.
37 Aggarwal M, Vij S & Kant N, *Optik*, 126 (2015) 5710.
38 Aggarwal M, Kumar H, Mahajan R, Arora N S & Gill T S, *Laser Part Beams*, 36 (2018) 353.
39 Vij S & Aggarwal M, *Commun Theor Phys*, 70 (2018) 317.
40 Khandale K Y, Takale P T, Patil S S, Nikam P P, Mane M B, Patil S D & Takale M V, *Indian J Pure Appl Phys,* 60 (2022) 967.
41 Takale P T, Khandale K Y, Nikam P P, Patil S S, Urunkar T U, Pawar V S, Patil S D & Takale M V, *Indian J Phys*, 97 (2023) 1849.
42 Khandale K Y, Takale P T, Patil S S, Urunkar T U, Patil S D & Takale M V, *Braz J Phys*, 53 (2023) 13.
43 Pawar V S, Kokare S R, Patil S D & Takale M V, *Laser Part Bemas*, 38 (2020) 204.
44 Pawar V S, Nikam P P, Kokare S R, Patil S D & Takale M V, *J Opt*, 50 (2021) 403.
45 Nikam P P, Pawar V S, Takale P T, Khandale K Y, Patil S S, Mane M B, Patil S D & Takale M V, *Indian J Pure Appl Phys*, 60 (2022) 576.
46 Bhatia A, Walia K & Singh A, *Optik*, 244 (2021) 167608.
47 Bhatia A, Walia K & Singh A, *Optik*, 245 (2021) 167747.
48 Kant N & Thakur V, *Chin J Phys*, 70 (2021) 182.
49 Wani M A & Kant N, *Optik*, 127 (2016) 4705.
50 Thakur V, Wani M A & Kant N, *Commun Theor Phys*, 71 (2019) 736.
51 Rui F, Zhang D, Ting M, Gao X & Zhuang S, *Optik*, 124 (2013) 2969.
52 Wang G, Miao Y, Li Y, Shan X & Gao X, *Chin Opt Lett*, 19 (2021) 022602.
53 Gawhary O E & Severini S, *J Opt A: Pure Appl Opt*, 8 (2006) 409.